Applied Catalysis B: Environmental 226 (2018) 616–623

Contents lists available at ScienceDirect

Applied Catalysis B: Environmental

journal homepage: www.elsevier.com/locate/apcatb

Self-assembled polymer phenylethnylcopper nanowires for photoelectrochemical and photocatalytic performance under visible light

Zhen Wei[a], Jisong Hu[b], Kaijian Zhu[c], Weiqin Wei[a], Xinguo Ma[b], Yongfa Zhu[a,*]

[a] Department of Chemistry, Tsinghua University, Beijing 100084, PR China
[b] School of Science, Hubei University of Technology, Wuhan 430068, PR China
[c] Key Laboratory of Flexible Electronics, Institute of Advanced Materials, Jiangsu National Synergetic Innovation Center for Advanced Materials, Nanjing Tech University, 30 South Puzhu Road, Nanjing 211816, PR China

ARTICLE INFO

Keywords:
Poly (phenylethynylcopper)
Metal organic polymers
Photocatalytic
Photoelectrochemical
Degradation phenolic compounds

ABSTRACT

PPECu nanowires were synthesized and the structure was explored. It was a metal organic polymer self-assembled by copper and phenylacetylene coordination and a p-type semiconductor material with the band gap of 2.48 eV. PPECu nanowires have excellent film-forming properties and exhibit hydrophobic properties. The photocurrent of PPECu was 10 times higher than that of g-C_3N_4 under the same conditions. The photoelectric conversion efficiency was 4.08% at 410 nm. It can activate molecular oxygen to produce superoxide radicals under visible light and the photocatalytic degradation of phenol and 2,4-DCP activity was 2.52 and 3.85 times higher than g-C_3N_4. Therefore, PPECu has a good potential at the application in the photoelectric conversion and photocatalytic degradation of pollutants.

1. Introduction

Increasing attention has been drawn on nanomaterials for photocatalytic or photoelectrochemical solar energy conversion to discover new methods for sewage purification and environmental protection [1–3]. The ultimate goal of catalysis is to optimize the use of solar energy. Therefore, the high efficient and stable photocatalysts that suitable for utilizing sunlight are required [4,5]. Metal oxide semiconductor photocatalysts (represented by titanium oxide) have been widely used in wastewater treatment and solar energy conversion over the past few decades [6,7]. The serious limitation of traditional inorganic photocatalysts (like TiO_2, ZnO and so on) [8,9] for applications is due to the low photoelectric conversion efficiency that results from the photogenerated electrons and holes easy to recombination and the large value of its bandgap which made it can only absorb ultraviolet irradiation [10,11]. In order to solve these problems, pure organic photocatalysts, including commonly reported carbon nitride [12], perylene-3,4,9,10-tetracarboxylic diimide [13] and some covalent organic polymers based on poly(p-phenylene) [14], poly(phenyleneethinylene) [15], poly(diphenylbutadiyne) [16], poly(azomethine) [17], and so on, which have been developed to tune the band structure to enhance the visible light absorption. However, the pure organic photocatalyst materials are subject to problems such as the limited of stability in use and also easy recombination of electrons and holes.

Metal organic polymers formed by the organic molecule in coordination with the metal ion. The metal atoms immobilized by coordinated with the organic molecule and the electronic structures tuned by self-assembly methods [18,19]. Metal organic polymer materials can expand the absorption of visible light and bridging ligands can form charge kinetics to promote the separation of photogenerated electrons and holes [4,20]. Metal organic polymers establish a connection point between traditional inorganic photocatalysts and pure organic photocatalysts materials [21]. Metal organic polymers are considered as promising energy conversion materials for applications in electrocatalysis, fuel cells, photodetectors, photovoltaic devices, and photocatalysts, due to their advantages of excellent electronic, optical properties and low-cost facile synthesis, high carrier mobility and diverse structural flexibility [22,23].

Due to the unique structural diversity of metal alkyne polymers, they have attracted a great deal of attention in the fields of novel electronic and optical materials [24–26]. Against this background, the metal alkyne polymers have many potential applications in photoelectric conversion and luminescence signal [27]. High-nuclearity metal alkyne clusters assembled with the C≡C− terminal of the alkynyl ligand to build the polymeric units [25,28]. Besides, the alkynyl ligand interacted with the transition metal through pπ–dπ making the alkynides can coordinate and bind to metals in diverse ways [29–31].

Polymer Phenylethnylcopper (PPECu) was studied focus on metal

* Corresponding author.
E-mail addresses: zhuyf@mail.tsinghua.edu.cn, zhuyf@tsinghua.edu.cn (Y. Zhu).

https://doi.org/10.1016/j.apcatb.2017.12.070
Received 27 November 2017; Received in revised form 23 December 2017; Accepted 29 December 2017
Available online 30 December 2017
0926-3373/

alkynes, mainly for copper-catalyzed alkyne–azide cycloaddition (CuAAC) reactions over the past few decades [32,33]. In this work, the hydrophobic PPECu nanowires were synthesized and the structure was explored. Series of photoelectric conversion performance tests showed that PPECu is a p-type semiconductor material with high response to visible light. The unique coordination polymer structure of PPECu make it has excellent thermal stability and rapidly separating photogenerated electron-hole under visible light. It can activate molecular oxygen to produce superoxide radicals under visible light and the photodegradation efficiency of phenol and 2,4-DCP activity was significantly better than g-C_3N_4. PPECu has a good potential at the application in the photoelectric conversion and photocatalytic degradation of pollutants.

2. Experimental section

All chemicals were analytically pure obtained from Sinopharm Chemical Reagent Corp, P. R. China and used without further purification.

2.1. Synthesis of $Cu_2(OH)_3OAc{\cdot}H_2O$

4 g $Cu(OAc)_2{\cdot}H_2O$ was dissolved in 200 mL deionized water at room temperature and stirred slowly added with 200 mL NaOH (0.1 M) solution. The mixed solution was stirred for 7 days. Washed several times, 60 °C vacuum drying 24 h.

2.2. Synthesis of PPECu

0.3 g $Cu_2(OH)_3OAc{\cdot}H_2O$ was dispersed in 50 mL methanol, and phenylacetylene (0.40 g) was added at 32 °C for 48 h. The product was centrifuged (5000 rpm, 5 min) and washed four times with water and ethanol respectively, then 60 °C vacuum drying 24 h.

2.3. Preparation of the PPECu thin film electrode

The working electrodes were prepared as follows: 5 mg of the as-prepared PPECu was dispersed in 1 mL ethanol to obtain a slurry. Then the slurry was dip-coated onto an indium tin oxide (ITO) glass (resistance: 30 Ω/square; size: 2 cm × 4 cm; thickness: 1.1 mm) electrode. Subsequently, the working electrodes were exposed to air atmosphere for 12 h to eliminate ethanol and dried at 80 °C in vacuo for 12 h.

2.4. Characterizations

The morphologies and structures of materials were measured by TEM operated on Hitachi HT 7700 at 100 kV. Details morphologies were observed by HRTEM on the JEM-2100F field emission high-resolution transmission electron microscope at 200 kV with high angle annular dark-field STEM. Field emission scanning electron microscopy (FESEM) was observed on a Hitachi SU-8010 at 10 kV. Powder X-ray diffraction was measured on Rigaku D/max-2400 with Cu Kα1 (λ = 1.5418 Å) radiation at 40 kV and 150 mA. The X-ray photoelectron spectra (XPS) were measured on a PHI Quantera SXM spectrometer using Al Ka radiation, and charging effect calibrated by the C 1 s peak at 284.8 eV. The UV–visible diffuse reflectance spectroscopy (DRS) of materials were carried out on Hitachi U-3010 spectrophotometer using $BaSO_4$ as a reference. Fourier transform infrared spectra (FT-IR) were taken on Bruker VERTEX-70 spectrometer from 4000 cm^{-1} to 600 cm^{-1} with the resolution of 1 cm^{-1}. Raman spectroscopy was recorded on a microscopic confocal Raman spectrometer HORIBA HR 800 with an excitation of the Ar^+ laser (514.5 nm). The room temperature photoluminescence (PL) spectra of materials were recorded on Perkin-Elmer LS55 spectrophotometer. Thermogravimetric analysis was obtained on Mettler Toledo TGA/DSC1 in the air with ten degrees per minute heating rate.

2.5. Photoelectrochemical measurements

The photoelectrochemical properties were evaluated in a conventional three-electrode cell system on CHI 660E (Shanghai, Chenhua) electrochemical workstation. PPECu film electrode as the working electrode, a saturated calomel electrode (SCE) as the reference electrode and a Pt wire used as the counter electrode. 0.1 M Na_2SO_4 aqueous solution was used as the electrolyte. To remove the dissolved oxygen, N 2 was bubbled into the Na2SO4 aqueous solution for 30 min before measurement. The working electrode was irradiated by a 500 W Xe lamp (Institute for Electric Light Sources, Beijing) and the light intensity was about 100 mW cm^{-2}. The linear sweep voltammogram (LSV) measurements scan rate was 10 mV s^{-1} at room temperature. The incident photon to-current efficiency (IPCE) was measured by a Xe lamp with different wavelengths obtained by band-pass filters. The power density of light source was measured by a photometer (Newport, USA).

The measurement system of steady-state surface photovoltage (SPV) was made-up as previously reported [34]. The monochromatic light resource was produced by a 500 W Xe lamp (CHF XQ500W) in conjunction with a double-prism monochromator (Omni-λ 3005) and the slit width was 3 mm. The samples were measured without further treatment and keep the contact was non-ohmic between the sample and the ITO electrode. The photovoltage signal was amplified by a lock-in amplifier (SR830-DSP) with a light chopper (SR540). The resolution of spectrum was 1 nm.

2.6. Photocatalytic degradation evaluation

The photocatalytic activity of PPECu was evaluated by the photodegradation efficiency of phenol and 2,4-DCP solution under the irradiation of visible light. The light source was provided by a Xe lamp at 500 W with 420 nm cutoff filter. The average light intensity was 22 mW cm^{-2}. The photodegradation reactions were measured in the quartz tube reactors with 20 mg as-prepared photocatalysts powders and 50 mL phenol or 2,4-DCP solution with a concentration of 5 ppm. The suspension solutions were first ultrasonically dispersed for 30 min in the dark and then stirred for 30 min before irradiation to reach the absorption–desorption equilibrium. At certain time intervals, 3 mL solution was sampled and centrifuged to remove the photocatalysts, and then filtrated with a 0.45 μm Millipore filter to remove the photocatalyst. The concentration of phenol and 2,4-DCP was analyzed by using the HPLC system (Shimadzu LC-20AT) with a C18 reversed phase column and an UV absorbance detector (K 2501). The determination wavelength was 270 nm (phenol) or 284 nm (2,4-DCP). The mobile phase was CH_3OH and H_2O (volume ratio: 60:40 (phenol) or 75/25 (2,4-DCP)) with a flow rate of 1 mL/min.

2.7. Theoretical calculations

All the theoretical work were accomplished by the Vienna Ab initio Simulation Package (VASP) version 5.4 in the MedeA® software environment [35]. The band gap and density of states (DOS) calculations were computed by the projector augmented wave (PAW) pseudopotentials with the correlation and exchange in the Perdew-Burke-Ernzerhof (PBE) [36] formalism of density functional theory (DFT) after the geometric optimization. A cutoff energy, Monkhorst–Pack k-mesh and the self-consistent convergence accuracy were set at 450 eV, 2 × 5 × 3 and 1 × 10^{-5} eV/atom, respectively [37]. The maximal force of the convergence criterion is 0.02 eV/Å. The stress is less than 0.02 Gpa, and the maximum displacement is 5 × 10^{-4} Å.

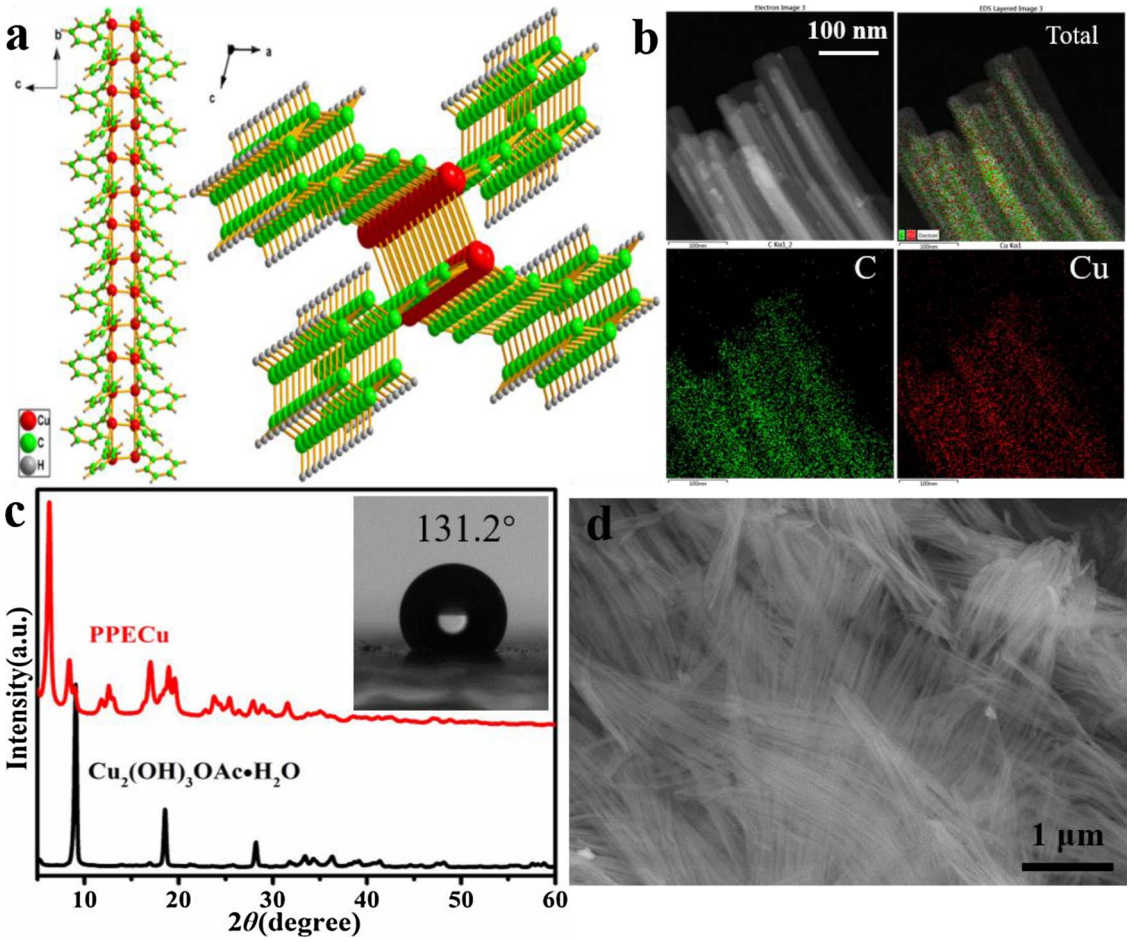

Fig. 1. a) schematic crystallographic structures of PPECu; b) STEM image of PPECu; c) XRD pattern of PPECu and $Cu_2(OH)_3OAc{\cdot}H_2O$, the inset picture was the static water droplet on PPECu; d) SEM image of PPECu.

3. Results and discussion

3.1. Morphology and structure of PPECu

PPECu nanowires were self-assembled by the coordination of copper and phenylacetylene. The $Cu_2(OH)_3OAc{\cdot}H_2O$ precursor was prepared with copper acetate as the raw material, and then PPECu nanowires were formed with phenylethylene (Fig. 1c). PPECu was the monoclinic phase, space group P 21 consistent with CCDC-242490 by X-ray diffraction (XRD) of PPECu nanowires (Fig. 1c). Polymer phenylethnylcopper crystal structure shown in Fig. 1a, from the a-axis direction, benzene acetylene along the Cu−Cu long chain on both sides of the distribution; Cu1 and Cu2 contributed a bridge of the same C≡C, Cu−Cu The distance between 2.49 (4) −2.83 (2) Å and Cu−C is 1.95 (1) −2.63 (1) Å, the distance between Cu−Cu bonds is less than the van der Waals radius of copper, indicating that there is a force between them, also shows that it is a chain structure by Cu and phenylacetylene coordination. From the direction of b-axis, it can be seen that π···π stack between phenylene diacetylene and self-assembled to nanowire structure. The PPECu dispersion has distinct Tyndall effect under a laser pan irradiation (Fig. S1), also indicating that it is a polymer instead of single molecule. From the SEM and TEM image (Figs. S2 and S3) can be seen PPECu was the nanowire structure, the width was about 20 nm and more than 1 μm long. It can be seen from the STEM (Fig. 1b) that only the Cu and C elements are evenly distributed on the nanowires (both the Cu and C elements and Cu and C are evenly distributed on the nanowires) from the light field and the energy spectrum. There is no obvious lattice image from the high-resolution TEM (HRTEM) images (Fig. S4), which may be due to the strong ability of the electron beam to penetrate the organic matter. From the photographs in the illustration (Fig. 4a inset), the sample was yellow powder, which can form a uniform film on ITO with excellent film-forming properties, and the measured contact angle is 131.2° (Fig. 1c inset), showing a strong hydrophobicity. The BET of PPECu specific surface area of 67.07 m^2/g (Fig. S6), aperture were 18.2 nm (Fig. S6) measured from N_2 isotherms indicating it has a certain adsorption properties.

In order to further analyze the composition of PPECu, it contains only Cu and C elements from the EDS test (Fig. S5). Thermogravimetric analysis and differential scanning calorimetry were conducted in the air atmosphere, PPECu was very stable in air below 170 °C from the TGA-DSC (Fig. 2a). PPECu has two exotherms at 230 °C and 300 °C oxidized by oxygen from DSC (Fig. 2a). Corresponding to the TGA, it can be seen at 230 °C has a weight loss about 26%, which is due to the partial oxidation of phenylacetylene; and at 300 °C have a larger weight loss about 56% owing to the complete oxidation of PPECu to cuprous oxide, calculated by the ratio of benzene acetylene and Cu was 1:1. This result is consistent with the composition of phenylacetylene copper.

The Raman spectrum of PPECu exhibits characteristic lines, which may be assigned to the benzene ring, at about 999, 1193 and 1599 cm^{-1} (Fig. 2b). Other lines (422, 529 cm^{-1}) are apparently due to vibrations involving predominantly copper and phenylacetylene coordination interaction. And 1971 cm^{-1} may be owing to a second-order transition enhanced by Fermi resonance with ν(C≡C) [38]. The absorption of 1927 cm^{-1} in the infrared spectrum (Fig. S8) is attributed to υ (C≡C−Cu): [39] It can be seen from the infrared spectrum that the absorption at 520 cm^{-1} attributed to Cu-ligand bond. PPECu have no absorption at 650 cm^{-1}(attributed to −C≡C−H) proving copper substituted for H completely [40].

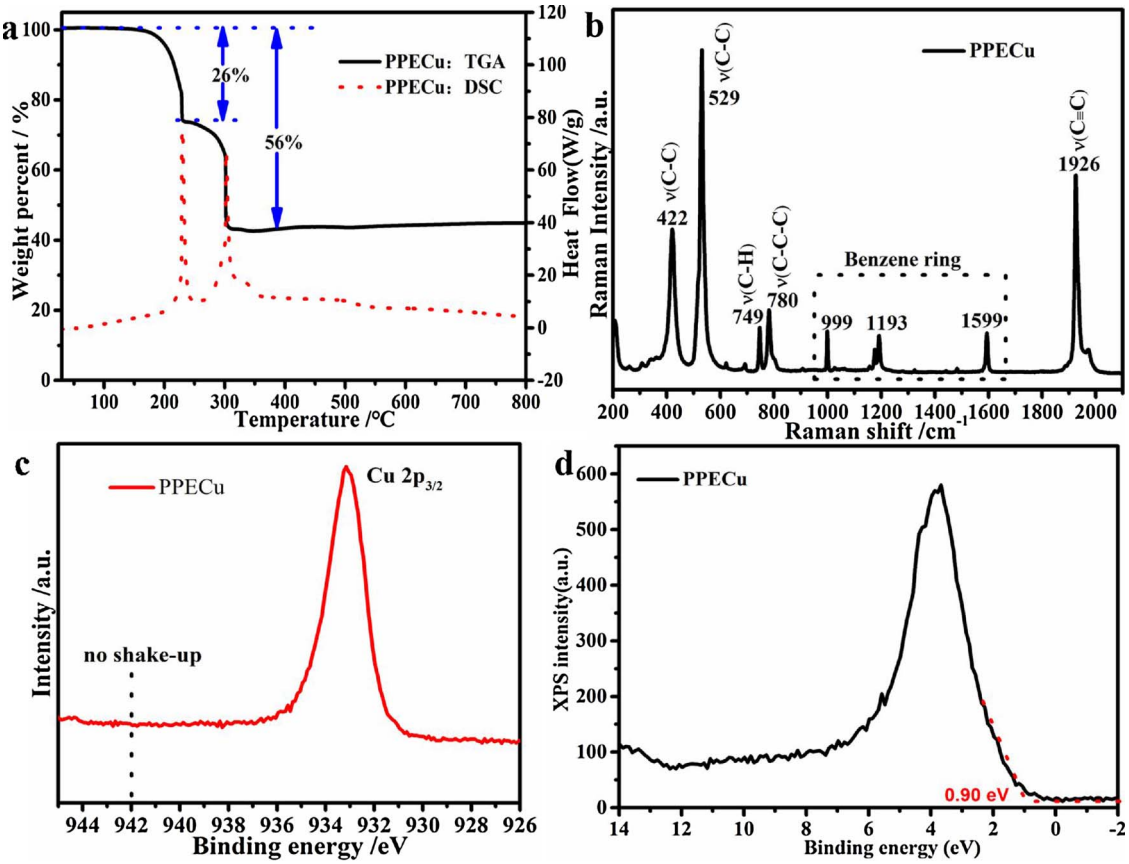

Fig. 2. a) TGA-DSC data of PPECu; b) Raman spectra of PPECu; c) The high-resolution XPS Cu spectrum of PPECu; d) The XPS valence band spectrum of PPECu.

The binding energy of Cu 2p1/2 was found at 933.0 eV is assigned to Cu^{+} (Figs. 2c and S13) [41]. No satellite peaks of Cu^{2+} are observed in the Cu 2p binding energy region indicating Cu of PPECu was +1 [42]. Due to coordinate with terminal alkynyl anions, Cu exhibits positive monovalent. From the XPS of the C 1 s spectrum(Fig. S12) can be seen with sp2, sp hybrid carbon, belonging to the carbon of PPECu on the benzene ring and alkene. It can be seen from XPS measurement that the copper of PPECu participates in coordination polymerization as monovalent.

3.2. Optical properties and band structure of PPECu

From the UV–vis diffuse reflection spectroscopy of PPECu (Fig. 3a), the absorption band was near 498 nm and the bandgap corresponds to 2.48 eV (see illustration). The PPECu valence band was at 0.90 eV from the XPS valence band spectrum (Fig. 2d), and it can be deduced that the conduction band is at −1.59 eV. While, it can be seen that the VB position is at 0.395 V from the cyclic voltammetry test, the conduction band should be at −2.095 V (Fig. S11). The UV–vis absorption of PPECu in ethanol was located at 365 and 467 nm corresponding to π-π* and d-π* (between Cu and the phenylethynyl group) charge transfer, respectively (Fig. 3c inset). The emission spectra of PPECu was at 435 nm and 519 nm, respectively, excited by excitation light at 325 nm (Fig. 3c). The emission band at 515 nm is attributed to a metal-perturbed ligand-centered π–π* (acetylide) emission. Besides, another distinctive band of higher energy at 410 nm also merges and may be assigned to intraligand π–π* emission of phenylacetylide [43].

To better understand the PPECu optical performance, the decay behavior of PPECu photoexcited carriers was investigated. Fig. 3d shows the time-resolved fluorescence emission decay spectra of PPECu monitored at 360 nm. The decay kinetics of PPECu is strikingly slow. In detail, the decay lifetime of carriers in PPECu is ca. 20.71 ns, indicating it has good separation efficiency of photoexcited charges and promote the PEC and photocatalytic activity [44,45].

To further uncover the correlation electron−hole separation efficiency of PPECu, steady-state surface photovoltage spectroscopy (SPV) as well as the phase spectra were conducted [46]. PPECu presents a strong negative photovoltage signal at 450 nm (Fig. 3b), indicating it has a high response to visible light and the holes are the main carriers. PPECu is a p-type semiconductor judging from the corresponding phase spectra were in the range of −90° to −180° (Fig. 3b inset) [46,47].

The photocatalytic activity of the PPECu is determined by the energy level and the band gap, which play a crucial role in semiconductor photocatalyst. The energy band diagram and density of states (DOS) of PPECu performed by density functional theory (DFT) as shown in Fig. 4a and b. The lowest unoccupied molecular orbitals (LUMO) and highest occupied molecular orbital (HOMO) isosurface with 0.04 of PPECu was shown in Fig. 4c and d. The occupied bands of PPECu were classified into two bands. The valence band (VB) mainly consists of Cu 3d + (alkynyl-) C 2p hybrid orbitals, the conduction band (CB) were mainly formed by the (phenyl-) C 2p + Cu 4p orbitals. The band gap of PPECu is estimated to be 1.707 eV, which was smaller than the obtained experimentally (2.48 eV). It should point out the common feature of DFT calculations failed to describe the excited states leading to underestimating the band gap. The band structure of PPECu presents that charge transfer upon photoexcitation occurs from the Cu 3d + (alkynyl-) C 2p hybrid orbitals to the (phenyl-) C 2p + Cu 4p hybrid orbitals.

3.3. Photoelectrocatalytic activity of PPECu

The photoelectrocatalytic performance was examined by measuring the current–voltage (*J–V*) curves under visible-light irradiation ($\lambda \geq 420$ nm, 100 mW cm^{-2}) with 0.1 M Na_2SO_4 aqueous solution (pH = 7) as the electrolyte. PPECu was coated on ITO glass and the

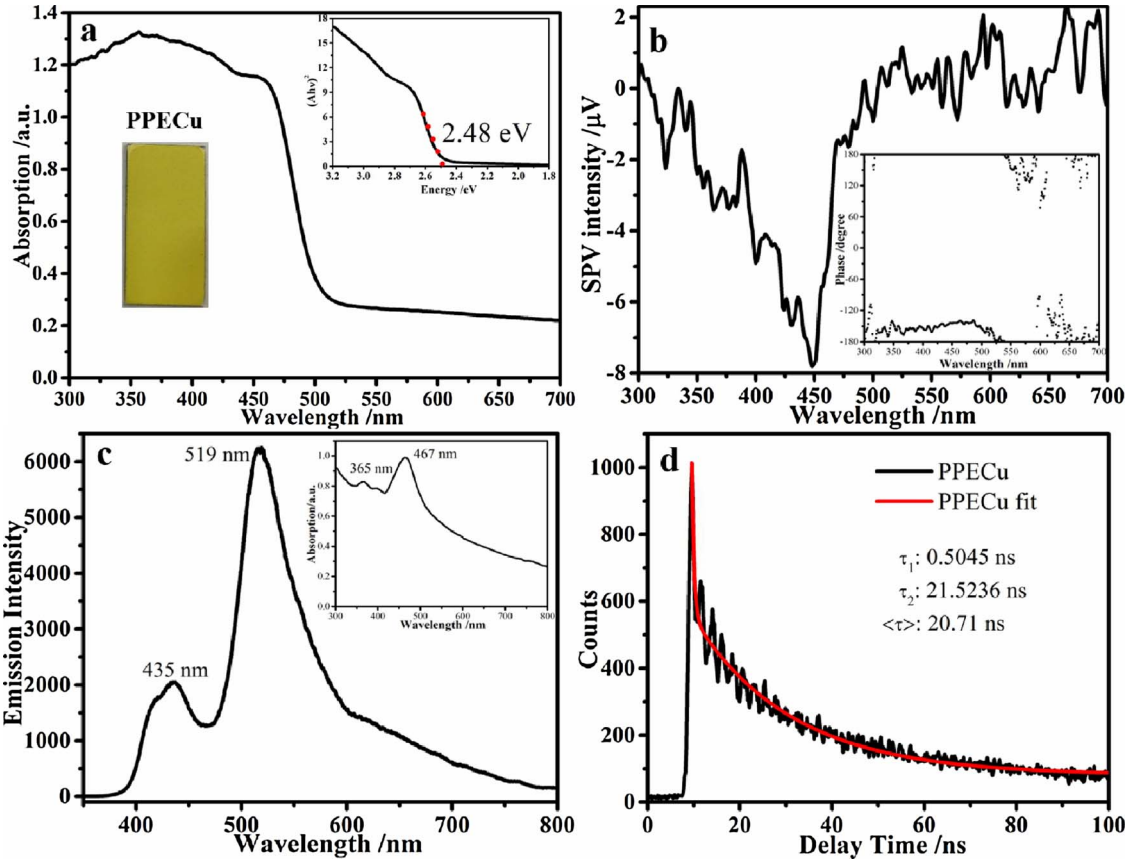

Fig. 3. a) DRS spectroscopy of PPECu and the inset picture was the optical photo of PPECu dipped on ITO; b) SPV spectrum of PPECu and (inset) corresponding phase spectra; c) PL spectrum of PPECu and UV–vis absorption spectra (inset) of PPECu; d) Room temperature time-resolved transient photoluminescence decays spectroscopy for the PPECu, excited at 360 nm.

photocurrent generated under visible light was 52 μA/cm^2, which is 10 times higher than that of g-C_3N_4 at the same condition (Fig. 5a). PPECu thin film exhibits cathodic photocurrent under visible-light illumination, which is similar to the photocurrent of p-type semiconductor Cu_2O [48,49]. PPECu shows great application potential for photoelectric conversion.

To further evaluate the activity of PPECu for photoelectrocatalytic, linear sweep voltammograms were obtained both in the dark and under light irradiation to show the *J–V* curves. With the applied bias, there is a significant increase in photocurrent. When the bias voltage is −0.05 V Vs. RHE, the photocurrent can reach 450 μA/cm^2 under AM1.5 light irradiation (Figs. 5b and S9). From the stability test of the photocurrent

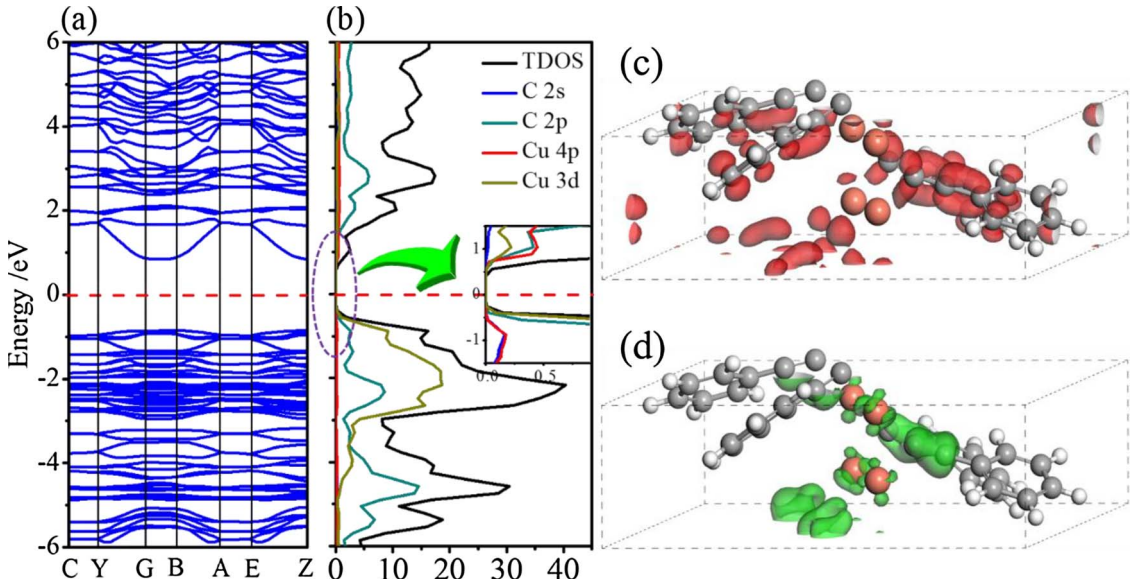

Fig. 4. Energy-band diagram (a) and density of states (b) for PPECu calculated by the DFT method. Fermi level is set to zero denoted as a red dashed line; The lowest unoccupied molecular orbitals (LUMO) (c) and highest occupied molecular orbital (HOMO) (d) isosurface with 0.04 of PPECu. White, Gray and brown spheres represent the H, C and Cu atoms, respectively. (For interpretation of the references to colour in this figure legend, the reader is referred to the web version of this article.)

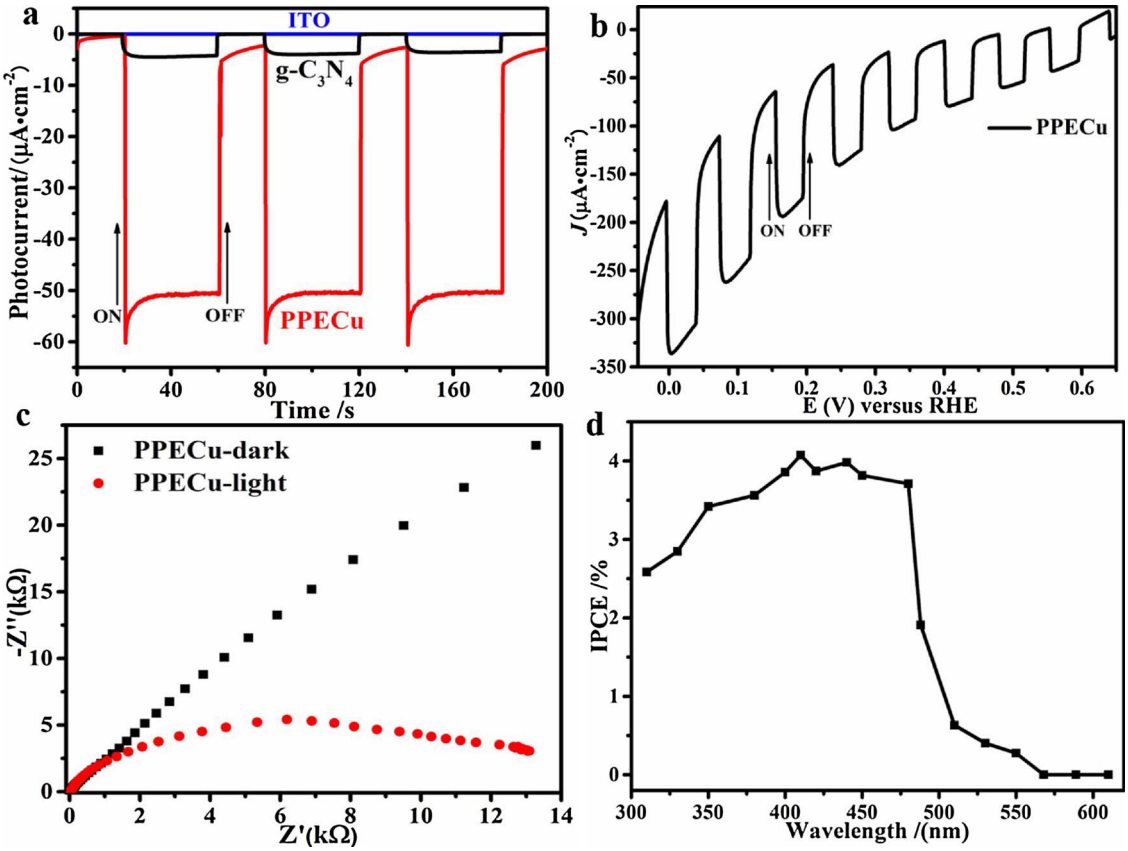

Fig. 5. a) Photocurrent density of PPECu, g-C_3N_4 and ITO film electrodes measured under visible-light illumination (λ > 420 nm); b) Linear sweep voltammograms curves under chopped visible-light irradiation (λ > 420 nm) for PPECu film electrodes in 0.1 M Na_2SO_4 aqueous solution; c) Electrochemical impedance spectroscopy Nyquist plots of PPECu; d) IPCE spectra of PPECu collected at 0 V_{RHE} under the AM 1.5G simulated sunlight (100 mW cm^{-2}) irradiation.

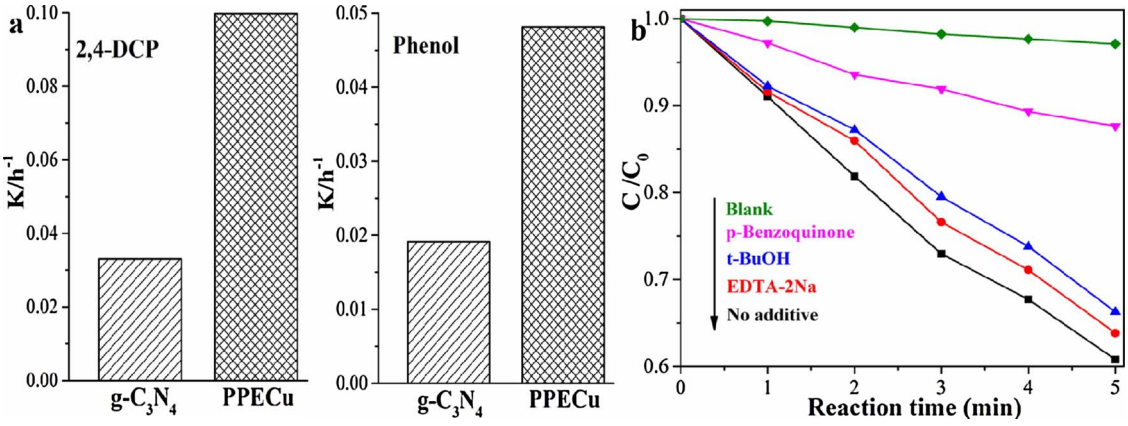

Fig. 6. a) The degradation rate constants for photocatalytic degradation of phenol and 2,4-DCP by g-C_3N_4, PPECu under visible light irradiation (λ > 420 nm); b) The trapping experiments of reactive species in degradation of 2,4-DCP by PPECu.

can be seen in the pressurized −0.05 V Vs. RHE light, 9000 s stable within the same (Fig. S10).

To further illustrate the interfacial charge-transfer property, electrochemical impedance spectroscopy (EIS) is employed [50,51]. The semicircular diameter of the Nyquist curve corresponds to the resistance of the charge transfer. From the A.C. impedance, it is significant that the resistance of PPECu under visible irradiation is quite less than no light conditions (Fig. 5c), the charge-transfer resistance (R_{ct}) of PPECu was calculated to be 209.31 kΩ under dark and 13.40 kΩ under visible light, indicating that the electron conductivity of the thin film photoelectrode was increased and visible light can increase the separation of photo-generated electrons and holes from PPECu.

Fig. 4d shows IPCE spectra of PPECu thin films photocathodes at 0 V RHE. IPCE of PPECu was about 4% from 410 to 480 nm and PPECu at 410 nm IPCE value of up to 4.08% (Fig. 5d). The IPCE dropped sharply from 480 nm to 510 nm. IPCE at 568 nm IPCE conversion value of 0 V, indicating that there is no photoelectric response. The IPEC result of PPECu was consistent with DRS and SPV results.

3.4. Photocatalytic activity of PPECu

Due to PPECu has an excellent visible light photoelectric response, photogenerated carriers can be well separated, it maybe has a good application on photocatalytic. The PPECu can be used as a visible-light active photocatalyst for photodegradation different kinds of pollutants. Phenolic compounds are a type of hard biodegradable hazardous waste.

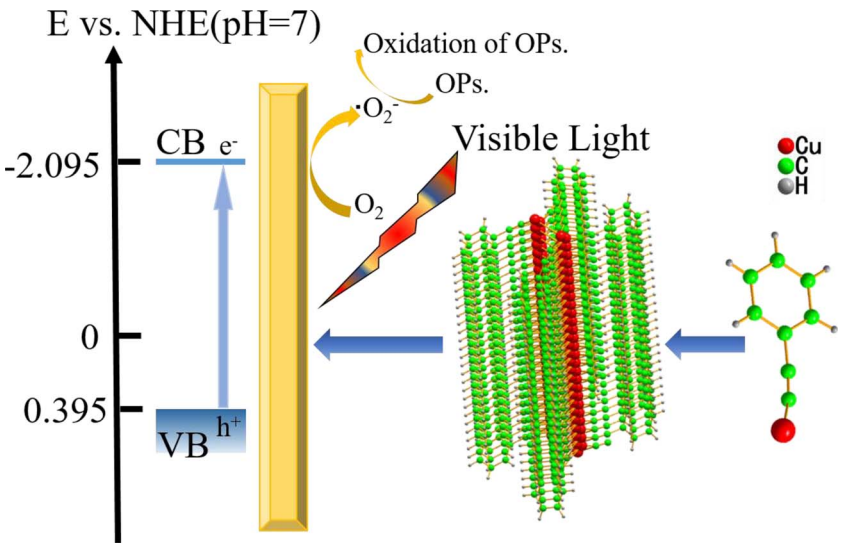

Scheme 1. The self-assembled of PPECu for nanowires and photocatalytic mechanism under visible light.

The environment has very stringent emission standards due to it highly toxic and persistent pollution [52,53]. The photocatalytic degradation of phenol and 2, 4-DCP was conducted to evaluate PPECu photocatalytic activity using g-C_3N_4 as the reference sample (Fig. 6a). The photocatalytic activity of PPECu was better than that of g-C_3N_4 under visible light by photocatalytic degradation of phenol and 2,4-DCP. The activity of 2,4-DCP was degraded by g-C_3N_4 as a reference is 3.85 times that of g-C_3N_4. The activity of PPECu degradation of phenol is 2.52 times of that of g-C_3N_4. To further evaluate the photocatalytic stability of PPECu, more times cyclic degradation experiments were measured (Fig. S14). It exhibited that there is hardly any obvious loss of photocatalytic activity after 4 cycles and the XRD (Fig. S15) was not changed, indicating that PPECu has a good stability on photocatalytic degradation. It may be owing to the strong coordination bond interaction between copper and phenylacetylene enhanced the stability of PPECu.

In order to further study the photocatalytic degradation mechanism, the active species trapping experiments were carried out using *tert*-butyl alcohol as hydroxyl radicals trapping agent, EDTA-2Na as the holes trapping agent, benzoquinone as superoxide radicals trapping agent (Fig. 6b) [54–56]. By adding different active species trapping agent, it was found that *p*-benzoquinone decreased the degradation rate most largely accordingly, indicating that the main active species were superoxide radicals. Phenylacetylene copper assembled into nanowires through coordination bonds, the formation of d-π conjugated system is easily excited by visible light to generate photo-generated electrons and holes (Scheme 1). The conduction band of PPECu is at −2.095 V and molecular oxygen is an acceptor of electrons (E (O_2/O_2^-) = −0.92 V [57]), the photogenerated electrons are generated when PPECu under visible light irradiation, molecular oxygen adsorbed on the surface of PPECu, the lone pair electrons of which conjugated with d orbit of copper, and the molecular oxygen is reduced to reactive oxygen species such as superoxide radicals to degrade the contaminants. Meanwhile, phenol and 2,4-DCP can be adsorbed on PPECu through the π-π interaction with phenylacetylene, accelerating the photocatalytic degradation. Due to the phenylacetylene intrinsic hydrophobic lead to PPECu also has a certain hydrophobicity, and PPECu has an excellent film-forming properties, which will have great potential value in self-cleaning materials application.

4. Conclusions

In conclusion, the PPECu nanowires were self-assembled by the coordination of copper and phenylacetylene. It was a metal organic polymer with the band gap of 2.48 eV p-type semiconductor material. PPECu nanowires have excellent film-forming properties and exhibit hydrophobic properties, which can apply in self-cleaning materials. The coordination between copper and phenylacetylene lead to superior visible-light-driven photoelectrochemical and photocatalytic performance. The photocurrent of PPECu was 10 times higher than that of g-C_3N_4 under the same conditions. The photoelectric conversion efficiency was 4.08% at 410 nm. It can activate molecular oxygen to produce superoxide radicals under visible light and the photocatalytic degradation of phenol and 2,4-DCP activity was 2.52 and 3.85 times higher than g-C_3N_4. Therefore, PPECu has a good potential at the application in the photoelectric conversion and photocatalytic degradation of pollutants. This work provides a new concept for design photocatalysis based on self-assembled metal organic polymers.

Acknowledgements

This work was partly supported Chinese National Science Foundation (21437003 , 21673126 , 21761142017 , 21621003 , 51472081) and Collaborative Innovation Center for Regional Environmental Quality.

Appendix A. Supplementary data

Supplementary data associated with this article can be found, in the online version, at https://doi.org/10.1016/j.apcatb.2017.12.070.

References

[1] N. Serpone, A.V. Emeline, J. Phys. Chem. Lett. 3 (2012) 673–677.
[2] D. Chen, K. Wang, W. Hong, R. Zong, W. Yao, Y. Zhu, Appl. Catal. B 166 (2015) 366–373.
[3] H. Yu, R. Shi, Y. Zhao, T. Bian, Y. Zhao, C. Zhou, G.I.N. Waterhouse, L.-Z. Wu, C.-H. Tung, T. Zhang, Adv. Mater. 29 (2017) 1605148–1605154.
[4] C. Gao, J. Wang, H. Xu, Y. Xiong, Chem. Soc. Rev. 46 (2017) 2799–2823.
[5] R. Shi, Y. Cao, Y. Bao, Y. Zhao, G.I.N. Waterhouse, Z. Fang, L.-Z. Wu, C.-H. Tung, Y. Yin, T. Zhang, Adv. Mater. 29 (2017) 1700803–1700809.
[6] L. Jing, W. Zhou, G. Tian, H. Fu, Chem. Soc. Rev. 42 (2013) 9509–9549.
[7] M. Pelaez, N.T. Nolan, S.C. Pillai, M.K. Seery, P. Falaras, A.G. Kontos, P.S. Dunlop, J.W. Hamilton, J.A. Byrne, K. O'shea, Appl. Catal. B 125 (2012) 331–349.
[8] J. Belloni, M. Treguer, H. Remita, R. De Keyzer, Nature 402 (1999) 865–867.
[9] Y. Zhao, B. Zhao, J. Liu, G. Chen, R. Gao, S. Yao, M. Li, Q. Zhang, L. Gu, J. Xie, Angew. Chem. Int. Ed. 55 (2016) 4215–4219.
[10] P.V. Kamat, J. Phys. Chem. Lett. 3 (2012) 663–672.
[11] J. Chen, D. Zhao, Z. Diao, M. Wang, S. Shen, Sci. Bull. 61 (2016) 292–301.
[12] X. Wang, K. Maeda, A. Thomas, K. Takanabe, G. Xin, J.M. Carlsson, K. Domen, M. Antonietti, Nat. Mater. 8 (2009) 76–80.
[13] D. Liu, J. Wang, X. Bai, R. Zong, Y. Zhu, Adv. Mater. 28 (2016) 7284–7290.
[14] T. Shibata, A. Kabumoto, T. Shiragami, O. Ishitani, C. Pac, S. Yanagida, J. Phys. Chem. 94 (1990) 2068–2076.
[15] D.-L. Jiang, C.-K. Choi, K. Honda, W.-S. Li, T. Yuzawa, T. Aida, J. Am. Chem. Soc. 126 (2004) 12084–12089.

[16] S. Ghosh, N.A. Kouamé, L. Ramos, S. Remita, A. Dazzi, A. Deniset-Besseau, P. Beaunier, F. Goubard, P.-H. Aubert, H. Remita, Nat. Mater. 14 (2015) 505–511.
[17] M.G. Schwab, M. Hamburger, X. Feng, J. Shu, H.W. Spiess, X. Wang, M. Antonietti, K. Müllen, Chem. Commun. 46 (2010) 8932–8934.
[18] H.Q. Pham, T. Mai, N.-N. Pham-Tran, Y. Kawazoe, H. Mizuseki, D. Nguyen-Manh, J. Phys. Chem. C 118 (2014) 4567–4577.
[19] G. Zhang, G. Kim, W. Choi, Energy Environ. Sci. 7 (2014) 954–966.
[20] P. Sippel, D. Denysenko, A. Loidl, P. Lunkenheimer, G. Sastre, D. Volkmer, Adv. Funct. Mater. 24 (2014) 3885–3896.
[21] H. Furukawa, K.E. Cordova, M. O'Keeffe, O.M. Yaghi, Science 341 (2013) 1230444.
[22] Y. Li, H. Xu, S. Ouyang, J. Ye, Phys. Chem. Chem. Phys. 18 (2016) 7563–7572.
[23] W.L. Leong, J.J. Vittal, Chem. Rev. 111 (2010) 688–764.
[24] H. Lang, D.S. George, G. Rheinwald, Coord. Chem. Rev. 206 (2000) 101–197.
[25] N.J. Long, C.K. Williams, Angew. Chem. Int. Ed. 42 (2003) 2586–2617.
[26] V.W.-W. Yam, J. Organomet. Chem. 689 (2004) 1393–1401.
[27] R. Buschbeck, P.J. Low, H. Lang, Coord. Chem. Rev. 255 (2011) 241–272.
[28] Y.-P. Xie, T.C. Mak, J. Clust. Sci. 25 (2014) 189–204.
[29] V.W.-W. Yam, C.-K. Hui, S.-Y. Yu, N. Zhu, Inorg. Chem. 43 (2004) 812–821.
[30] C.E. Powell, M.P. Cifuentes, J.P. Morrall, R. Stranger, M.G. Humphrey, M. Samoc, B. Luther-Davies, G.A. Heath, J. Am. Chem. Soc. 125 (2003) 602–610.
[31] S.-K. Yip, C.-L. Chan, W.H. Lam, K.-K. Cheung, V.W.-W. Yam, Photochem. Photobiol. Sci. 6 (2007) 365–371.
[32] B.R. Buckley, S.E. Dann, H. Heaney, Chem. Eur. J. 16 (2010) 6278–6284.
[33] B.R. Buckley, S.E. Dann, D.P. Harris, H. Heaney, E.C. Stubbs, Chem. Commun. 46 (2010) 2274–2276.
[34] H. Fan, H. Li, B. Liu, Y. Lu, T. Xie, D. Wang, ACS Appl. Mater. Interfaces 4 (2012) 4853–4857.
[35] G. Kresse, J. Hafner, J. Phys. Condens. Matter. 6 (1994) 8245.
[36] J.P. Perdew, K. Burke, M. Ernzerhof, Phys. Rev. Lett. 77 (1996) 3865.
[37] H.Y. Jiang, P. Zhou, Y. Wang, R. Duan, C. Chen, W. Song, J. Zhao, Adv. Mater. 28 (2016) 9776–9781.
[38] I. Garbusova, V. Alexanjan, L. Leites, I. Golding, A. Sladkov, J. Organomet. Chem. 54 (1973) 341–344.
[39] Y. Okamoto, S.K. Kundu, J. Phys. Chem. 77 (1973) 2677–2680.
[40] H. Krikor, M. Rotti, P. Nagels, Synth. Met. 21 (1987) 353–359.
[41] Y. Xie, A. Riedinger, M. Prato, A. Casu, A. Genovese, P. Guardia, S. Sottini, C. Sangregorio, K. Miszta, S. Ghosh, J. Am. Chem. Soc. 135 (2013) 17630–17637.
[42] Z. Guan, W. Luo, J. Feng, Q. Tao, Y. Xu, X. Wen, G. Fu, Z. Zou, J. Mater. Chem. A 3 (2015) 7840–7848.
[43] S.S. Chui, M.F. Ng, C.M. Che, Chem. Eur. J. 11 (2005) 1739–1749.
[44] M.Y. Ye, Z.H. Zhao, Z.F. Hu, L.Q. Liu, H.M. Ji, Z.R. Shen, T.Y. Ma, Angew. Chem. Int. Ed. 56 (2017) 8407–8411.
[45] G. QingáLu, Chem. Commun. (2009) 3452–3454.
[46] H. Fan, D. Wang, L. Wang, H. Li, P. Wang, T. Jiang, T. Xie, Appl. Surf. Sci. 257 (2011) 7758–7762.
[47] T. Ivanov, V. Donchev, K. Germanova, K. Kirilov, J. Phys. D Appl. Phys. 42 (2009) 135302.
[48] A. Paracchino, V. Laporte, K. Sivula, M. Grätzel, E. Thimsen, Nat. Mater. 10 (2011) 456–461.
[49] T. Baran, S. Wojtyła, C. Lenardi, A. Vertova, P. Ghigna, E. Achilli, M. Fracchia, S. Rondinini, A. Minguzzi, ACS Appl. Mater. Interfaces 8 (2016) 21250–21260.
[50] B. Klahr, S. Gimenez, F. Fabregat-Santiago, J. Bisquert, T.W. Hamann, J. Am. Chem. Soc. 134 (2012) 16693–16700.
[51] C. Li, Y. Li, J.-J. Delaunay, ACS Appl. Mater. Interfaces 6 (2013) 480–486.
[52] Z. Wei, F. Liang, Y. Liu, W. Luo, J. Wang, W. Yao, Y. Zhu, Appl. Catal. B 201 (2017) 600–606.
[53] Q. Hao, S. Hao, X. Niu, X. Li, D. Chen, H. Ding, Chin. J. Catal. 38 (2017) 278–286.
[54] Z. Wei, D. Liu, W. Wei, X. Chen, Q. Han, W. Yao, X. Ma, Y. Zhu, ACS Appl. Mater. Interfaces 9 (2017) 15533–15540.
[55] Q. Hao, X. Niu, C. Nie, S. Hao, W. Zou, J. Ge, D. Chen, W. Yao, Phys. Chem. Chem. Phys. 18 (2016) 31410–31418.
[56] Q. Hao, R. Wang, H. Lu, W. Ao, D. Chen, C. Ma, W. Yao, Y. Zhu, Appl. Catal. B 219 (2017) 63–72.
[57] L.E. Manring, M. Kramer, C.S. Foote, Tetrahedron Lett. 25 (1984) 2523–2526.